Journal of Quantitative Spectroscopy & Radiative Transfer ▮ (▮▮▮▮) ▮▮▮–▮▮▮

Contents lists available at SciVerse ScienceDirect

Journal of Quantitative Spectroscopy & Radiative Transfer

journal homepage: www.elsevier.com/locate/jqsrt

Interaction of optical Whispering Gallery Modes with the surface layer of evaporating droplet of suspension

M. Kolwas, D. Jakubczyk *, G. Derkachov, K. Kolwas

Institute of Physics of the Polish Academy of Sciences, Al.Lotników 32/46, 02-668 Warsaw, Poland

ARTICLE INFO

Article history:
Received 31 October 2012
Received in revised form
15 February 2013
Accepted 5 March 2013

Keywords:
Whispering Gallery Modes
Micro-cavities
Droplet with inclusions
Nano-particles aggregate
Evaporation driven phenomena
Interference image analysis

ABSTRACT

We investigate scattering of light on micro droplets of suspensions of 100-nm and 225-nm-radius dielectric spheres in glycols. Rapid increase of scattered light intensities accompanied by light depolarisation was observed on presumed formation of the surface layer of inclusions. We determined the effective refractive index of the droplet (surface) evolving during the formation of the surface layer of inclusions. We present a model enabling identification of interaction of surface structures of inclusions with Whispering Gallery Modes of the droplet. It seems possible to exploit the evaporation of micro droplets of suspension as a method of production of composite objects with very specific indices of refraction.

1. Introduction

The optical properties of a droplet of suspension containing small, sub-micron particles [1] can well depend on such properties of these particles as their dimension, shape or distribution. In the simplest case, the effective (optical) properties of a composite object are a simple volume fraction mixture of components' properties [2]. However, in many cases such approach is oversimplified. In particular, optical properties of an evaporating droplet of suspension can be strongly modified by formation of the surface layer of inclusions [3], since the vicinity of the droplet surface is occupied by the relevant optical modes of the droplet. The total field interacting with a (surface layer) inclusion consists of incident field, field scattered on the droplet as a whole (effective refractive index) and field scattered by other inclusions. The interaction of this total field with inclusions structures manifests in a complex way. The influence of the surface layer of inclusions (structures) on Whispering Gallery Modes (WGM) of the droplet seems particularly important. The concept of WGM can be clearly grasped with the Mie theory [4]. It has been developed under different names (morphology resonances [5], partial wave resonances, structural resonances [6,7]), etc. WGM appears in the context of ultra-sensitive detection [8], micro-cavities [9,10] and micro-lasers [11] as well. In this paper we try to analyse the influence of the surface layer of inclusions, forming on evaporating droplet of suspension, on the process of light scattering on such a droplet. In particular, we pursue the interaction with WGM. We minimised the influence of inclusions distributed in droplet volume by employing suspensions of low refractive index difference between components. It is worth noticing, that the surface roughness is known to enhance various optical phenomena due to enhancement of the local field [12].

2. Scattering by a micro-droplet containing inclusions

Scattering on a spherically symmetric, homogeneous and optically linear droplet can be described with Mie theory. In

* Corresponding author. Tel.: +48 22 116 29 91.
E-mail address: jakub@ifpan.edu.pl (D. Jakubczyk).

0022-4073/$ - see front matter © 2013 Elsevier Ltd. All rights reserved.
http://dx.doi.org/10.1016/j.jqsrt.2013.03.009

order to describe scattering of light on a micro-droplet of suspension, apart from scattering on a droplet-sized sphere, the scattering on inclusions should be considered. We treat scattering on inclusions as an additional source of scattering on a composite droplet. This simple attitude is justified by the observed order of optical phenomena during evaporation of a droplet of suspension with small initial fraction of inclusions. First we observe Mie scattering typical for homogeneous sphere with well-pronounced Whispering Gallery Modes (WGM), then we see a sudden appearance of additional modes of scattering caused by inhomogeneities forming in observed object. This simple model serves to understand, classify and qualitatively describe the phenomena observed in our experiments rather than to quantitatively model scattering of light on non-homogeneous particle.

In our experiments, the refractive indices of inclusions (polystyrene 100-nm-radius nano-spheres: $n_{D20}=1.58$; SiO_2 225-nm-radius nano-spheres: $n_{D20}=1.46$) were nearly equal to those of the liquids (ethylene glycol (EG): $n_{D20}=1.43$, diethylene glycol (DEG): $n_{D20}=1.45$) and the surface active agent (sodium dodecyl sulphate (SDS)): $n_{D20}=1.46$. Therefore the droplet of suspension can be treated as optically homogeneous and scattering of light on inclusions can be neglected as long as they stay beneath the droplet surface. When inclusions appear at the surface they scatter light as separate objects [13].

The electric field of scattered light is proportional to the incident field E_I at the position of scatterer

$$\vec{E}_{sca} \propto e^{i\vec{q}\cdot\vec{r}}\,\vec{E}_I \tag{1}$$

where $q=2k\sin(\theta/2)$, θ is the scattering angle and k is the incident wave number.

Thus, the scattering on N scatterers can be written as

$$I(q)\propto\left|\sum_{i=1}^{N} e^{i\vec{q}\cdot\vec{r}}\,\vec{E}_I(\vec{r}_i)\right| = \sum_{i}^{N}\sum_{j}^{N} e^{i\vec{q}\,(\vec{r}_i-\vec{r}_j)}\,\vec{E}_I(\vec{r}_i)\,\vec{E}^{*}_I(\vec{r}_j) \tag{2}$$

where $\vec{r}_i$ and $\vec{r}_j$ are the positions of ith and jth scatterer respectively.

Scatters distributed on the droplet surface interact with a local field composed of the incident (laser) field $\vec{E}_0$ and the field scattered on the droplet $\vec{E}_d$. Therefore:

$$\vec{E}_I(\vec{r}_i)=\vec{E}_0(\vec{r}_i)+\vec{E}_d(\vec{r}_i) \tag{3}$$

If the droplet is much larger than the wavelength and the distribution of inclusions is random, the scattering is incoherent, i.e. only terms with $i=j$ in Eq. (2) contribute. As the liquid evaporates and the distances between inclusions shrink the coherent scattering terms with $i\neq j$ come into play. In order to extract the properties of coherent and incoherent scattering we introduce the surface density function (number per unit area) of inclusions $\rho(\vec{r})$ enabling to replace summation with integration

$$\rho(\vec{r})=N^{-1}\sum_{i=1}^{N}\delta(\vec{r}-\vec{r}_i)\quad\text{and}$$

$$\sum_{i=1}^{N} e^{i\vec{q}\cdot\vec{r}_i}=N\int e^{i\vec{q}\cdot\vec{r}}\,\rho(\vec{r})\,d\vec{r}, \tag{4}$$

where δ is the Dirac delta function. Then

$$\sum_{i\neq j}^{N}\sum_{j}^{N} e^{i\vec{q}\,(\vec{r}_i-\vec{r}_j)}\,\vec{E}_s(\vec{r}_i)\,\vec{E}^{*}_s(\vec{r}_j)\cong\left|N\int e^{i\vec{q}\cdot\vec{r}}\,\rho(\vec{r})\,d\vec{r}\right|^2, \tag{5}$$

where $E_s=E_0,E_d$ and

$$\sum_{i=1}^{N}|\vec{E}_d(\vec{r}_i)|^2=N\int\rho(\vec{r})|\vec{E}_d(\vec{r})|^2 d\vec{r}. \tag{6}$$

Eq. (2) can be transformed into the following form (see e.g. [13] p. 656):

$$I(q)\cong I_{incoh}(q)+I_{coh}(q), \tag{7}$$

where

$$I_{incoh}(q)\cong N\sigma\left(I_0+\int\rho(\vec{r})|\vec{E}_d(\vec{r})|^2 d\vec{r}\right) \tag{8}$$

$$\begin{aligned} I_{coh}(q)\cong\sigma\Bigg(&\left|N\int e^{i\vec{q}\cdot\vec{r}}\,\rho(\vec{r})\,\vec{E}_0(\vec{r})d\vec{r}\right|^2\\ &+\left|N\int e^{i\vec{q}\cdot\vec{r}}\,\rho(\vec{r})\,\vec{E}_d(\vec{r})d\vec{r}\right|^2\Bigg)\\ &=I_{coh^A}(q)+I_{coh^B}(q)\end{aligned} \tag{9}$$

and

$$\sigma=k^4a^6\left|\frac{n^2-1}{n^2+2}\right|^2. \tag{10}$$

The incoherent term I_{incoh} consists of two parts: (i) proportional to the number of scatterers (inclusions) only and (ii) proportional to the convolution of the surface density of inclusions and the field scattered by the droplet. The coherent term I_{coh} also consists of two parts: I_{coh^A} proportional to the coherent scattering of laser light on inclusions and I_{coh^B} proportional to coherent convolution of the surface density of inclusions and the field scattered by the droplet. We neglected the interference terms E_0E_d, since these fields travelling along entirely different optical paths have much different phases.

$\vec{E}_d(\vec{r})$ can be calculated with Mie theory (see e.g. [14]). It should be stressed that for large droplets (droplet radius much larger than the light wavelength $R\gg\lambda$) the presence of Whispering Gallery Modes is clearly pronounced in the scattered light intensity. There is an extensive literature on WGM as spherical micro-cavity modes [15,16]. For the purpose of this work, for the sake of simplicity, we will approximate WGM as standing waves along the droplet equator with maxima corresponding to $R_{max}=m\lambda/(2\pi n)$, where m is an integer number. Consequently, the spacing, along the droplet equator, between the maxima of scattered light intensity associated with WGM is λ/n. Thus, the field amplitude associated with WGM at the droplet surface can be simulated in a very simple way:

$$E_{WGM}=E\cos(\kappa R)\sin(\kappa L), \tag{11}$$

where $\kappa=m/R_{max}$, L is the coordinate along the droplet equator and $\langle x\rangle$ is the mean distance between inclusions. The $\sin(\kappa L)$ term describes the distribution of WGM field (standing wave) along the equator.

Please cite this article as: Kolwas M, et al. Interaction of optical Whispering Gallery Modes with the surface layer of evaporating droplet of suspension. J Quant Spectrosc Radiat Transfer (2013), http://dx.doi.org/10.1016/j.jqsrt.2013.03.009

It seems reasonable to assume Gaussian distribution of inclusions on the droplet surface, so also along the equator we get

$$\rho(\delta L) = \frac{1}{w\sqrt{2\pi}} \exp\left[-\frac{(\delta L - \langle x\rangle)^2}{2w^2}\right], \tag{12}$$

where w is the standard deviation of the distribution and δL describes the distance from the density maximum.

Thus the integrals in Eq. (8) can be estimated along the equator and I_{incoh} takes a perspicuous form:

$$I_{incoh}(q) \cong 1 + \tfrac{1}{2}\cos^2(\kappa R)[1 - W\cos(2\kappa\langle x\rangle)], \tag{13}$$

where $W \propto \exp(-2\kappa^2 w^2)/(w\sqrt{2\pi})$. We do not put equality here since in general a WGM maximum may not coincide with the density maximum. It can be readily noticed that the intensity of I_{incoh} oscillates with radius R and is additionally modulated as $\cos(2\kappa\langle x\rangle)$.

When inclusions are close enough or form a regular pattern on the surface they scatter light coherently (Eq. (9)). The maxima of I_{coh^A} correspond to resonances associated with fitting of mean distance $\langle x\rangle$ to the light wavelength. They disappear when the distribution of x becomes too wide, i.e. qw is large.

$$I_{coh^A}(q) \cong \left|\frac{NE_0}{w\sqrt{2\pi}} \exp\left(\frac{-q^2w^2}{2}\right)\exp(\imath\langle x\rangle q)\right|^2. \tag{14}$$

I_{coh^B} term describes the interference of the above described local resonances and WGM (being nonlocal resonances).

$$I_{coh^B}(q) \cong \frac{NE_0\cos(\kappa R)}{2w\sqrt{2\pi}} \sum_{z=\pm 1} \exp\left[-\frac{(q+z\kappa)^2w^2}{2}\right]\exp(\imath q\langle x\rangle) \times \exp(\imath z\kappa\langle x\rangle). \tag{15}$$

It may be difficult to distinguish all kinds of resonances in real experiment observation. But careful separation of them can give deep insight into surface phenomena.

3. Experimental apparatus and sample preparation

Schematic drawing of the experimental setup and the outline of data processing procedures is presented in Fig. 1. Single droplets of suspension were levitated in an electrodynamic quadrupole trap (built in our lab; cutaway drawing presented in the centre of Fig. 1). Electrodynamic trapping is a well-established experimental technique, see e.g. [17–25]. A particular combination of alternating (AC) and static (DC) electric fields, in (close to) quadrupolar configuration, enables constraining particle(s) to a small volume of "free" space, ideally to a point. Particle(s) of a certain charge to mass ratio q/m sit then in the pseudo-potential minimum formed by oscillating saddle-shaped field. Trajectories of a particle in oscillating, quadrupolar field can be described with Mathieu equations. The trap was kept in a small ($\sim$10 cm^3) thermostatic chamber with dry nitrogen atmosphere at 25 °C and atmospheric pressure. Droplets were injected into the trap with the droplet-on-demand injector (built in our lab as well; similar to e.g. [26,27]) kept at chamber temperature. The droplets were charged by charge separation in the external field of the trap, on emerging from the injector nozzle (no additional charging electrodes were used). Thus, the sign and the value of the charge was, to some extent, determined by the injection timing versus the phase of the trapping AC field. Our setup allows stable trapping of droplets from $\sim$35 μm down to $\sim$0.5 μm radius. The average initial droplet radius is several μm. Two coaxial, counter propagating laser beams were used simultaneously for droplet illumination: green (532.07 nm, 5.5 mW)

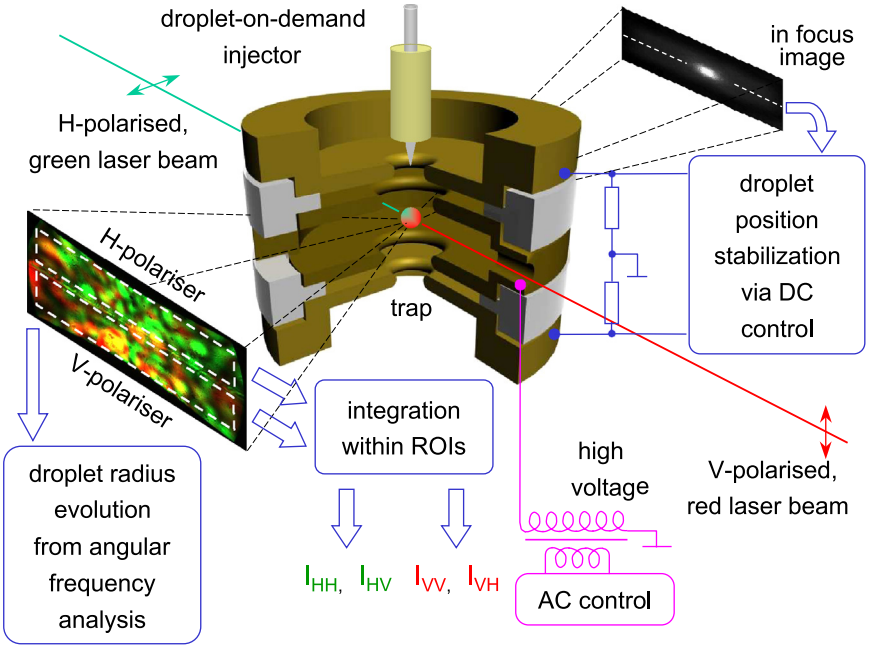

Fig. 1. Schematic drawing of experimental setup and the outline of the data processing procedures. Cutaway drawing of the electrodynamic quadrupole trap together with the droplet-on-demand injector shown in the centre. Droplet presented as 100 × oversized.

Please cite this article as: Kolwas M, et al. Interaction of optical Whispering Gallery Modes with the surface layer of evaporating droplet of suspension. J Quant Spectrosc Radiat Transfer (2013), http://dx.doi.org/10.1016/j.jqsrt.2013.03.009

H-polarised (horizontal) and red (654.25 nm, 10 mW) *V*-polarised (vertical). The focused image of the droplet collected with a microscope and a simple B/W camera was used for droplet position stabilisation. The vertical position of the (evaporating) droplet was maintained at the trap centre with a PID type stabilising loop, applying a balancing DC voltage between the top and bottom electrode. Analysing the temporal evolution of this DC voltage enables, in combination with scatterometry, weighting of the droplet. No secular (macro) motion was allowed or observed. In lateral directions, non-absorbing droplets performed only trap-constrained Brownian motions. Neither photophoresis nor thermophoresis nor radiation pressure effects were observed. Simultaneously, the droplet was in the focus of lens with NA=0.28 with axis at the right angle in the horizontal scattering plane. The entirely defocused images of the droplet, registered with the colour CCD camera (PixelFly, pco.imaging), was used for scatterometry. The distortions of frequency and shape of the interference fringes/speckles (spherical aberration and other geometrical effects) were corrected numerically in post-processing. Two linear polarisers were used in the detection channel: *H*-polariser (in respect to the scattering plane; upper half of the channel) and the *V*-polariser (the lower half of the channel). Using a colour camera allowed us to separate spectrally the elastically scattered light and attribute it to appropriate incident beam polarisation. We recorded temporal evolution of the intensity distributions of the scattered light of the same polarisation as the polarisation of the incident light (of a given colour) ($I_{VV}(\Theta,t)$ and $I_{HH}(\Theta,t)$), and the cross-polarised (depolarised) light intensities ($I_{VH}(\Theta,t)$ and $I_{HV}(\Theta,t)$) correspondingly.

In experiments presented in this work we generated droplets of suspensions: (i) 100-nm-radius polystyrene (PS; Thermo Scientific, 3200A) nano-spheres in diethylene glycol (DEG; Fluka, BioUltra, 99.99 GC area %) with sodium dodecyl sulfate (SDS; Sigma-Aldrich, ACS Reagent, ≥99.0%), (ii) 225-nm-radius silica (SiO_2, C-SIO-0.45, Corpuscular) micro-spheres in DEG with SDS and (iii) 225-nm-radius SiO_2 micro-spheres in ethylene glycol (EG; SPECTRANAL, Riedel-de Haën, 99.9 GC area %) with SDS. The suspensions were prepared by first mixing EG or DEG with SDS and then with pre-concentrated suspension of PS or SiO_2 nano-spheres in water and sonicating. The approximate initial mass fractions were: (i) PS:SDS:DEG=2:1:1000, (ii) SiO_2:SDS:DEG=2:1:500 and (iii) SiO_2:SDS:EG=10:1:2000. After the injection of a micro-droplet into the dry-nitrogen atmosphere, the water fraction evaporates in a fraction of the first second (compare [25,28]) leaving the desired suspension.

The bulk properties of substances used in experiments are presented in Table 1.

The temporal evolution of the droplet radius $R(t)$, was obtained with a combination of methods consisting of scatterometry and weighting [32] assisted by analysis of WGM position. Scatterometry analyses angular distribution of scattered light intensity (angle-resolved static light scattering, see eg. [33] and references therein) for every acquired frame. The method variant that we developed belongs to a group of look-up table methods which rely on comparing experimentally obtained versus theoretically predicted scattering patterns. Weighting enables retrieving of the droplet radius as long as the density of droplet material is known. Since during evaporation all solid inclusions stay in the droplet/composite agglomerate, the changes of droplet density can be accounted for. Supplementing the results of scatterometry/weighting combination with the Mie theory based analysis of WGM temporal positions seen in the scattered light intensity enables further improvement of radius measurement. An example of $R(t)$ is presented in Fig. 2.

Table 1
Refractive index and density of substances used in experiments @ 25°. n_{D20} values provided by the manufacturers of the chemicals. The n_{D20} for SDS is 1.46. Dispersion curve for PS nano-spheres taken from [29] and for EG from [30]. The dispersion curves for SiO_2 micro-spheres and for DEG were adapted from [31] (fused silica) and from [30] (EG) respectively.

Substance	Density (kg/m^3)	Refractive index @	
		532.07 (nm)	654.25 (nm)
Ethylene glycol (EG)	1109	1.432	1.429
Diethylene glycol (DEG)	1114	1.448	1.445
Polystyrene (PS) nanospheres	1050	1.588	1.582
Silica (SiO_2) microspheres	1700	1.461	1.457

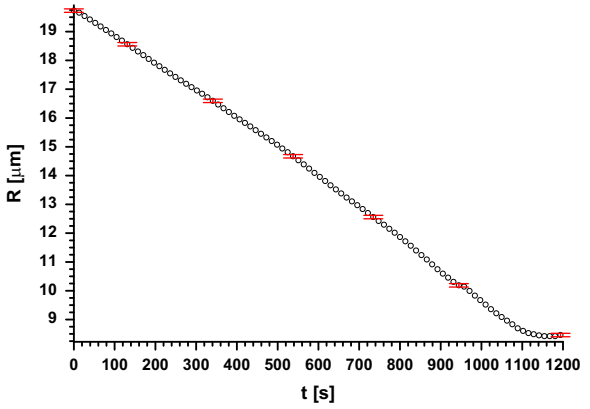

Fig. 2. Temporal evolution the droplet radius, corresponding to Figs. 4–6. Open circles represent radius obtained with scatterometry/weighting combination (only every 400th point shown). Circle size corresponds to estimated radius measurement accuracy; error bars for radius shown (in red) for selected data points correspond to WGM maxima spacing; uncertainty of temporal position was negligible. (For interpretation of the references to color in this figure caption, the reader is referred to the web version of this article.)

4. Interaction of WGM with droplet surface layer of 100-nm-radius inclusions

In our experiment we observe scattered light intensity integrated over elevation angle Φ from −5 to 5 degrees and azimuthal angle Θ from 70 to 110 degrees in scattering plane. For a homogeneous sphere such intensity can be calculated with the Mie theory. A manifold of WGM resonances, calculated with the Mie theory for *VV* and *HH* polarisations, is presented in Fig. 3 as a function of droplet radius.

Please cite this article as: Kolwas M, et al. Interaction of optical Whispering Gallery Modes with the surface layer of evaporating droplet of suspension. J Quant Spectrosc Radiat Transfer (2013), http://dx.doi.org/10.1016/j.jqsrt.2013.03.009

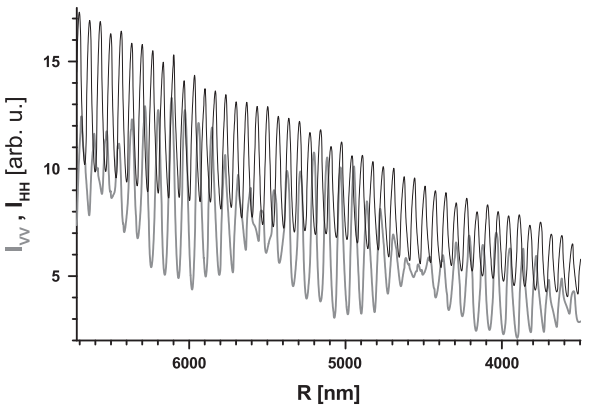

Fig. 3. Theoretical I_{VV} (grey) and I_{HH} (black) scattered light intensities calculated with the Mie theory (integrated over observation angles to meet the experimental conditions) for $n=1.4$. The high frequency oscillations correspond to WGMs. The modulation of I_{VV} can be perceived in the frame of Debye's series as the partial waves interference (see eg. [34,35]). The steady increase of both I_{VV} and I_{HH} intensities versus radius is the manifestation of geometrical cross-section increase.

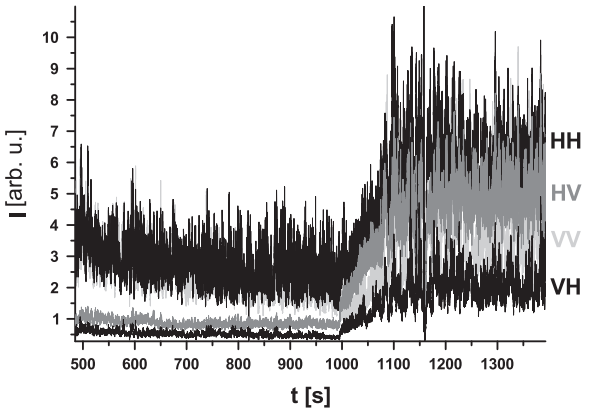

Fig. 4. Intensity of scattered light on all 4 polarisation combinations. The rapid increase of scattered light intensity begins when the inclusions start to accumulate at the droplet surface at ~1000 s. The stabilisation of (average) intensity of scattering signals marks the end of intensive evaporation.

In the experiments with droplets of suspension of 100-nm-radius PS nano-spheres in DEG, we observed similar signal until the moment in which the scattering on inclusions appeared (Fig. 4).

As it has been already mentioned, because of small difference between refractive indices of DEG and PS, only the inclusions located at the surface and in contact with air scatter intensively, which leads to light depolarisation. In this way crossed-polarised signals I_{VH} and I_{HV} appear. It should be emphasised that observation of cross-polarised signals carries information on inclusions (surface roughness). After ~ 1000 s of evolution the growing intensity of scattering indicates the formation of inclusion's layer(s) on the surface. After ~1200 s the droplet should be rather perceived as an agglomerate particle. As it can be seen in Fig. 2, its radius ceases to change or changes very slowly (drying porous material, compare [36]) then. This coincides with stabilisation of (average) magnitude of scattering signals.

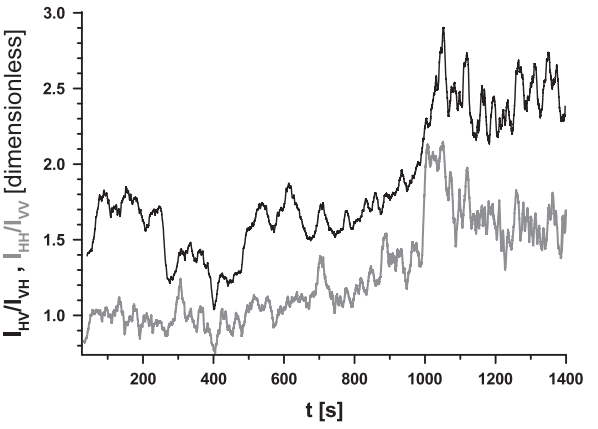

Fig. 5. The ratios of signals of straight polarisations I_{HH}/I_{VV} (grey) and cross-polarisations I_{HV}/I_{VH} (black). (For interpretation of the references to color in this figure caption, the reader is referred to the web version of this article.)

It can be noticed (Fig. 5) that the ratio between I_{HH} (green laser light) and I_{VV} (red laser light) signal grows over time until the beginning of formation of inclusions layer at the surface (at ~1000 s). Then the ratio reaches its maximum value of ~2. This suggests Rayleigh scattering proportional to k^4 (compare Eq. (10) and $N\sigma I_0$ term in (8)), i.e. on separate objects smaller than light wavelength ($a=100$ nm in this case). The decrease which follows indicates the growing influence of scattering on larger objects, e.g. growing aggregates. The cross-polarised intensities ratio I_{HV}/I_{VH}, after an initial increase, stabilises. This suggests the saturation of number of surface inclusions.

It is possible, by studying scattering signals in fine detail, to point to some phenomena concerning the formation of inclusions surface layer. We shall illustrate it by analysing the I_{VH} (red) cross polarised light (Fig. 6). It begins to vary from 995 s of droplet evolution. After relatively smooth first short stage (995–1000 s) the intensity starts to oscillate regularly (see Fig. 6). The Whispering Gallery Modes can be identified by comparing experimental results with the Mie theory calculations (see inset in Fig. 6 and compare Eq. (8)). We interpret it as due to the interference of WGM with surface structure of inclusions, which is described with cos $(2\kappa\langle x\rangle)$ term in Eq. (13). It should be remembered that mean distance between inclusions $\langle x\rangle$ is a function of droplet radius and therefore of time.

In the evolution that follows, the character of resonances changes which can be associated with formation of more compact two dimensional structure of inclusions (a surface aggregate). The beating of WGM structure is covered by a manifold of resonances due to the interference of light scattered on different inclusions (structures). This phenomenon is described with I_{coh^A} term in Eq. (9). This contribution to scattering is additive to incoherent one and does not originate from interference with WGM-s. It seems realistic to assume that in this region WGM-s disappear due to the collapse of the regular surface structure.

5. Properties of surface layer

It seems possible to evaluate, at least qualitatively, the properties of the surface layer of inclusions when it is

Please cite this article as: Kolwas M, et al. Interaction of optical Whispering Gallery Modes with the surface layer of evaporating droplet of suspension. J Quant Spectrosc Radiat Transfer (2013), http://dx.doi.org/10.1016/j.jqsrt.2013.03.009

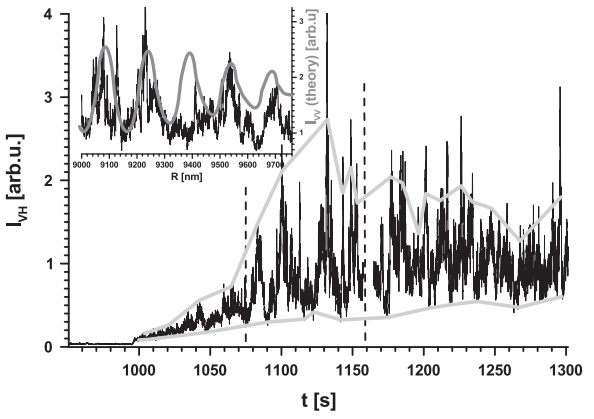

Fig. 6. The intensity of depolarised light I_{VH} in the region of strong scattering. First I_{VH} grows as the number of inclusions accumulated at the surface increases, than it starts to oscillate due to the interaction of the surface structure of inclusions with WGM of the droplet. The WGM can be identified by comparing experimental I_{VH} with the Mie theory calculations for I_{VV} (inset, gray). Inset corresponds to region marked in main figure with vertical dashed lines. The base line and amplitude of WGM modulation marked with light gray solid lines.

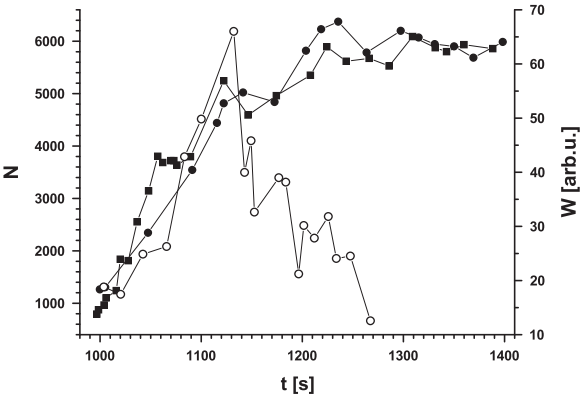

Fig. 7. The number of inclusions calculated from minima of I_{VV} (solid squares) and I_{HH} (solid circles) respectively. Open circles: evolution of W.

regular enough not to destroy WGM of the droplet. We study 3 properties of the $I_{VH}(t)$ signal (Fig. 6): (i) the base line of modulation, (ii) the amplitude A of modulation and (iii) the positions of WGM resonances. The relative number of inclusions located on the droplet surface can be directly inferred from the base line of modulation (see grey line in Fig. 6) by means of Eq. (8). Finding the actual number N of inclusions on the surface requires calibration. To this end, we note that when the mean distance between inclusions approach the light wavelength in the medium (compare Eq. (13)), the amplitude of modulation is highest. The gauging equation takes then a simple form

$$0.74N(A = A_{max})\langle x\rangle^2 = 4R^2. \tag{16}$$

It should be underlined, that the close-packing arrangement (the factor of 0.74) corresponds, counter-intuitively, to the average distance between inclusions and not to inclusions in direct contact. In case of DEG, the vacuum wavelength of 654 nm (red light) is reduced to 453 nm in the medium ($n = 1.445$, see Table 1) and for data presented in Fig. 6 we find

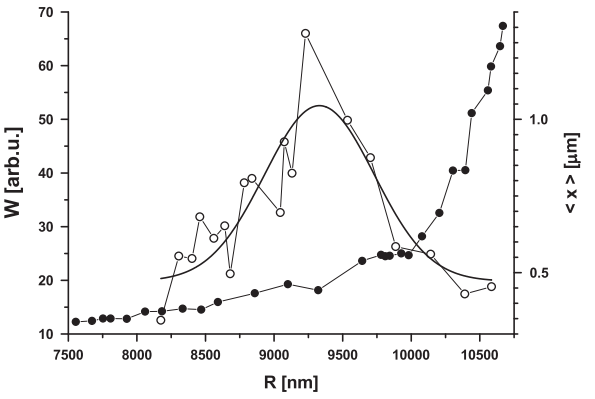

Fig. 8. The temporal evolution of W (open circles) and the mean distance of inclusions $\langle x\rangle$ (solid circles). Gaussian profile fit to $W(R)$ represented by solid line.

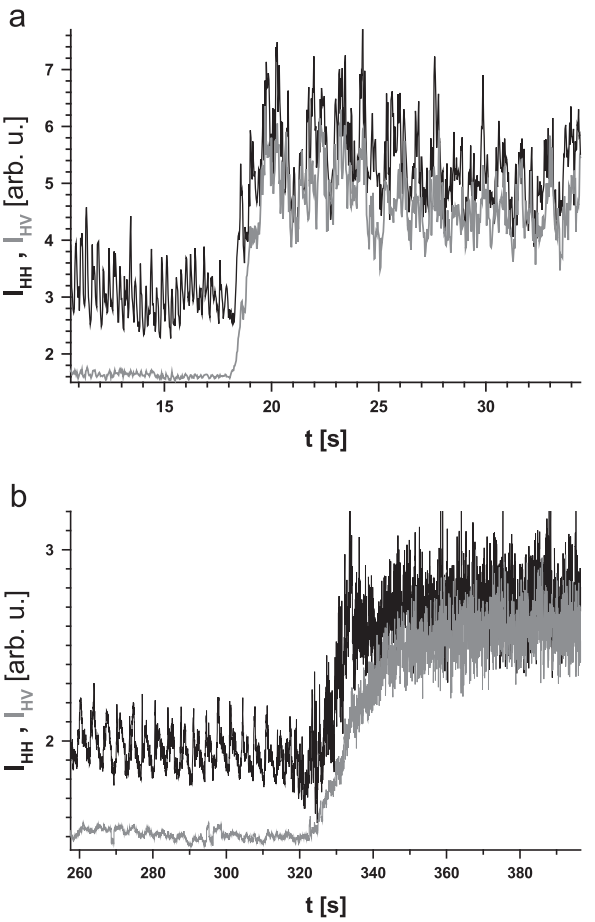

Fig. 9. Examples of scattered light intensities for evaporating droplets of suspensions of SiO_2 in liquids of different volatility: (a) EG and (b) DEG. The intensities of straight-polarised scattered light, represented by I_{HH} (black line) in both figures, are modulated due to WGM and decrease proportionally to the surface area of the droplet until the formation of the surface layer of inclusions. The intensities of cross-polarised light, represented by I_{HV} (gray line) in both figures, are nearly constant until the surface layer of inclusions formation.

Please cite this article as: Kolwas M, et al. Interaction of optical Whispering Gallery Modes with the surface layer of evaporating droplet of suspension. J Quant Spectrosc Radiat Transfer (2013), http://dx.doi.org/10.1016/j.jqsrt.2013.03.009

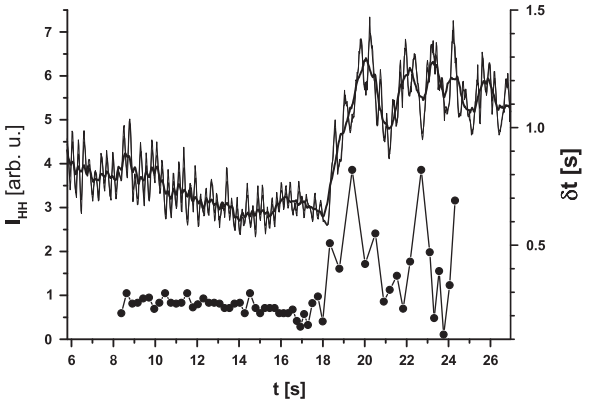

Fig. 10. Upper curve: I_{HH} signal close to the formation of the surface layer of inclusions (smoothed signal superimposed). Lower curve (solid circles): the temporal evolution of the interval δt between WGM maxima (measured from the raw signal).

$N(t=1130)=4920$ nm. Using WGM resonance position for gauging allows us to expect that the accuracy of $N(A=A_{max}$ (number scaling) should be better than 1%. Since the droplet radius at modulation maximum can be determined ± 1 distance between WGM maxima, which is ~60 nm, the accuracy of $N(A=A_{max}$ is $\pm$~30 inclusions. However, the main source of uncertainty of $N(t)$ is the determination of the baseline value. Judging by the discrepancy between results obtained from I_{VV} and I_{HH} (Fig. 7) this uncertainty should not be larger than 25%.

In order to find a parameterisation of the distribution of distances between inclusions x, we use the parameter $W=A/N$ which can be perceived as a surface inclusions order parameter. The temporal evolution of W found from experimental data and the mean distance of inclusions $\langle x\rangle$ are shown in Fig. 8. During the evaporation of liquid from the droplet, W increases first, reaching the highest value at 1132 s (narrowest mean distance distribution), and then decreases. The dependence of W upon droplet radius has resonant character.

The amplitude A depends on competition of WGM resonator quality (amount of energy stored at the surface) and the efficiency of scattering of WGMs on inclusions distributed on the surface. This competition can be seen in Fig. 7: W is maximal before the number of surface inclusions reaches maximum.

6. Effective index of refraction of surface layer: inclusions SiO_2, $a=225$ nm

In order to study the properties of surface layer in detail we used larger inclusions of SiO_2 ($a=225$ nm) suspended in DEG and in much more volatile EG. In spite of significant difference in evaporation rate we observed similar phenomena (see Fig. 9). At early stage of evaporation oscillations associated with WGMs were clearly pronounced, indicating optical homogeneity and spherical shape of the droplet. Then a rapid increase of scattered light intensities was observed suggesting the surface layer of inclusions formation. That was followed by saturation of scattering signals with oscillations superimposed, indicating transition of the surface layer of inclusions into a multi layer aggregate and then into an aggregate of less regular structure of the surface. Very similar effects were observed in case of 100-nm-radius inclusions.

However, in case of SiO_2 inclusions additional small maximum appears few seconds before rapid growth of all intensities. It is especially well pronounced for suspension in EG between 15 and 18 s in I_{HH} signal in Fig. 9(a). This effect seems to be connected with interaction of light with under-surface inclusions, since it is absent in depolarised signals (see I_{HV} in Fig. 9). This maximum is accompanied by a slight decrease of distance δt between WGM resonances (measured from raw signal; shown in Fig. 10). It is followed by a rapid growth of δt, in the evolution range identified as the surface layer formation, starting at ~18 s. The manifestation of WGM depends on the local quality of the resonator. The effective refractive index of the droplet surface can be perceived as some measure of this quality. Thus its value may be somewhat misleading. We use the distance between two WGM maxima $\delta R=\lambda/(2\pi n)$ to estimate the effective index of refraction of the droplet surface (Fig. 11). We assume that the initial refractive index at the surface is identical with the initial bulk refractive index, which is known. Since the character of the droplet radius evolution is very similar to that presented in Fig. 2, for short intervals $\delta t\propto\delta R$. This approximation holds for any short interval, perhaps except the very "kink" at the end agglomerate formation. The value of n grows from the 15th s of evaporation, suggesting that under the smooth surface of the droplet (no cross-polarised I_{HV} or I_{VH} signals) some inclusions structure is formed. Then, at ~18 th s, cross-polarisation signals appear and begin to grow. Simultaneously, the index of refraction decreases as low as 0.5. We attribute this effect to interaction of WGMs with surface inclusions. The formation of inclusions structure on the droplet surface (a meta material layer) influences the position of resonances associated with WGM. This can be observed as a modification of the effective refractive index of the droplet surface.

After the rapid increase (after 20th s in Fig. 10), the scattered light intensity begins to oscillate slowly (in respect to WGM resonances). This modulation seems to be related to the evolution of the mean distance between inclusions $\langle x\rangle$ in respect to the wavelength. Since the

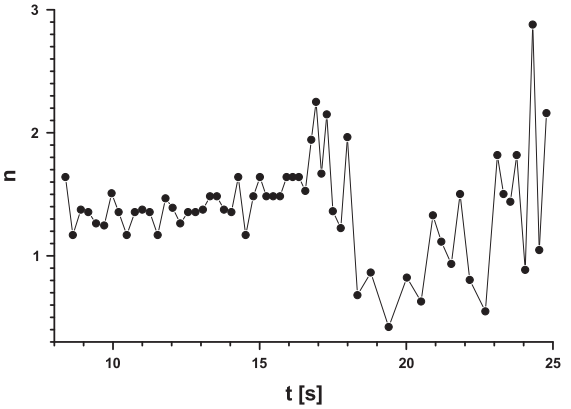

Fig. 11. The effective index of refraction of the droplet surface calculated from the intervals between WGM maxima.

Please cite this article as: Kolwas M, et al. Interaction of optical Whispering Gallery Modes with the surface layer of evaporating droplet of suspension. J Quant Spectrosc Radiat Transfer (2013), http://dx.doi.org/10.1016/j.jqsrt.2013.03.009

inclusions are larger ($a=225$ nm) the beats are slower than in case of 100-nm-diameter inclusions.

7. Conclusions

In our experiments on drying droplets of suspensions we observed rapid increase of scattered light intensities and appearance of scattered light depolarisation. We associate it with a sudden formation of surface layer of inclusions. We have presented a simple description making it possible to identify interactions of surface inclusions and their structures with Whispering Gallery Modes of the droplet. The formation of surface layer seems very promising not only as a vehicle for studying the dynamics of evaporation but also as means for engineering spherical aggregates of desired index of refraction. In particular such aggregates can serve as micro-cavities of designed properties.

Acknowledgments

This work was supported by Polish Ministry of Science and Higher Education under grant No N N202 126837 and by the Ministry of Science and Higher Education/European Science Foundation (ESF/PESC EPSD program) as a scientific project 2010-2013.

References

[1] Doyle W. Optical properties of a suspension of metal spheres. Phys Rev B 1989;39(14):9852–8. http://dx.doi.org/10.1103/PhysRevB.39.9852.
[2] Kreibig U, Vollmer M. Optical properties of metal clusters. Berlin: Springer; 1995.
[3] Jakubczyk D, Kolwas M, Derkachov G, Kolwas K. Surface states of microdroplet of suspension. J Phys Chem C 2009;113(24):10598602. http://dx.doi.org/10.1021/jp9007812.
[4] Mie G. Beiträge zur optik trüber medien, speziell kolloidaler metallösungen. Ann d Phys 1908;25:377–445.
[5] Mishchenko M, Lacis A. Manifestations of morphology-dependent resonances in Mie scattering matrices. Appl Math Comput 2000;116(1–2):167–79.
[6] Chylek P, Kiehl J, Ko M. Optical levitation and partial waves resonances. Phys Rev A 1978;18:2229–33.
[7] Datsyuk V, Izmailov I. Optics of microdroplets. Phys-Usp 2001;44(10):1061–73.
[8] Vollmer F, Arnold S. Whispering-gallery-mode biosensing: label-free detection down to single molecules. Nat Methods 2008;5:591–6.
[9] Vahala K. Optical microcavities. Nature 2003;424:839–46. http://dx.doi.org/10.1038/nature01939.
[10] Kavokin A, Baumberg J, Malpuech G, Laussy F. Microcavities series on semiconductor science and technology. OUP Oxford; 2007.
[11] Tona M. Study on spherical microlasers levitated in ion trap. PhD thesis. Kochi University of Technology; 2002.
[12] Boyd G, Rasing T, Leite J, Shen Y. Local-field enhancement on rough surfaces of metals, semimetals, and semiconductors with the use of optical 2nd-harmonic generation. Phys Rev B 1984;30:519–26.
[13] Sorensen C. Light scattering by fractal aggregates: a review. Aerosol Sci Tech 2001;35:648–87.
[14] Bohren C, Huffman D. Absorption and scattering of light by small particles. New York: Wiley; 1998.
[15] Matsko A, Savchenkov A, Strekalov D, Ilchenko V, Maleki L. Review of applications of whispering-gallery mode resonators in photonics and nonlinear optics. IPN Prog Rep 2005;42–162:1–51.
[16] Righini G, Dumeige Y, Féron P, Ferrari M, Nunzi Conti G, Ristic D, et al. Whispering gallery mode microresonators: fundamentals and applications. Riv Del Nuovo Cimento 2011;34(7):435–88. http://dx.doi.org/10.1393/ncr/i2011-10067-2.
[17] Paul W. Electromagnetic traps for charged and neutral particles. Rev Mod Phys 1990;62:531–40.
[18] Major F, Gheorghe V, Werth G. Charged particle traps. Berlin: Springer; 2005.
[19] Davis E, Buehler M, Ward T. The double-ring electrodynamic balance for microparticle characterization. Rev Sci Instrum 1990;61(4):1281–8.
[20] Arnold S. A three-axis spherical void electrodynamic levitator trap for microparticle experiments. Rev Sci Instrum 1991;62(12):3025–8.
[21] Shaw R, Lamb D. Experimental determination of the thermal accommodation and condensation coefficients of water. J Chem Phys 1999;111:10659–63.
[22] Allison E, Kendall B. Cubic electrodynamic levitation trap with transparent electrodes. Rev Sci Instrum 1996;67(11):3806–12.
[23] Itoh M, Arakawa E, Sakiyama K, Tanaka K, Takano H. Manipulation of a single aerosol particle in a quadrupole cell by dual-sided invisible laser irradiation. J Aerosol Sci 1999;30(Suppl. 1):S403–4.
[24] Heinisch C, Wills J, Reid J, Tschudi T, Tropea C. Temperature measurement of single evaporating water droplets in a nitrogen flow using spontaneous Raman scattering. Phys Chem Chem Phys 2009;11:9720–8. http://dx.doi.org/10.1039/b908555f.
[25] Jakubczyk D, Derkachov G, Do-Duc T, Kolwas K, Kolwas M. Coefficients of evaporation and gas phase diffusion of low-volatility organic solvents in nitrogen from interferometric study of evaporating droplets. J Phys Chem A 2010;114(10):3483–8. http://dx.doi.org/10.1021/jp911466e.
[26] Ulmke H, Wriedt T, Bauckhage K. Piezoelectric droplet generator for the calibration of particle-sizing instruments. Chem Eng Technol 2001;24(3):265–8.
[27] Lee E, Perl M. Universal Fluid Droplet Ejector; 1999. U.S. Pat. No. 5943075.
[28] Wilms J. Evaporation of multicomponent droplets. PhD thesis. Universität Stuttgart; 2005.
[29] Ma X, Lu J, Brock R, Jacobs K, Yang P, Hu X. Determination of complex refractive index of polystyrene microspheres from 370 to 1610 nm. Phys Med Biol 2003;48:4165–72.
[30] El-Kashef H. The necessary requirements imposed on polar dielectric laser dye solvents. Physica B 2000;279:295–301. http://dx.doi.org/10.1016/S0921-4526(99)00856-X.
[31] Leviton D, Frey B. Temperature-dependent absolute refractive index measurements of synthetic fused silica. Proc SPIE 2006; 6273, 62732K. http://dx.doi.org/10.1117/12.672853.
[32] Jakubczyk D, Derkachov G, Kolwas M, Kolwas K. Combining weighting and scatterometry: application to a levitated droplet of suspension. J Quant Spectrosc Radiat Transfer 2012. http://dx.doi.org/10.1016/j.jqsrt.2012.11.010.
[33] Dehaeck S, van Beeck J. Multifrequency interferometric particle imaging for gas bubble sizing. Exp Fluids 2008;45(5):823–31. http://dx.doi.org/10.1007/s00348-008-0502-8.
[34] Hovenac E, Lock J. Assessing the contributions of surface waves and complex rays to far-field Mie scattering by use of the Debye series. J Opt Soc Am A 1992;9(5):781–95.
[35] Albrecht HE, Damaschke N, Borys M, Tropea C. Laser doppler and phase doppler measurement techniques. Berlin: Springer; 2003.
[36] Davies J, Haddrell A, Miles R, Bull C, Reid J. Bulk, surface, and gas-phase limited water transport in aerosol. J Phys Chem A 2012;116(45):10987–98. http://dx.doi.org/10.1021/jp3086667.

Please cite this article as: Kolwas M, et al. Interaction of optical Whispering Gallery Modes with the surface layer of evaporating droplet of suspension. J Quant Spectrosc Radiat Transfer (2013), http://dx.doi.org/10.1016/j.jqsrt.2013.03.009